Extent of back diffusion during solidification of experimental nickel based single crystal superalloy

A. Thirumalai[1], A. Akhtar[1] and R. C. Reed*[2]

The microsegregation inherited from the directional solidification and quenching (DSQ) of an experimental third generation single crystal superalloy is characterised using electron probe microanalysis (EPMA). A statistical treatment of the data is used to estimate the composition of the solid in the mushy zone. Comparison of the experimental data with the predictions from a numerical model indicates that the results cannot be rationalised without acknowledging that back diffusion is occurring; it is demonstrated that the magnitudes of the diffusion coefficients which need to be invoked are consistent with recent experimental measurements of the coefficients deduced from diffusion couples.

Keywords: Superalloys, Solidification, Diffusion, Transformation mechanism

Introduction

The nickel based superalloys are a category of material which have been developed specifically for high temperature applications, e.g. for the turbine blades and nozzle guide vanes required for the gas turbine engine.[1] Investment casting using directional solidification process[2] is the manufacturing route of choice, because it allows components to be fabricated of complex geometry with serpentine cooling passages inside them; therefore, they are usually hollow with wall thicknesses as small as a few millimetres. Furthermore, the components are often cast into single crystal form using a grain selector or else a seeding technique. This situation – together with the strict requirement for defect free castings on account of the mechanical integrity required during engine operation – presents a significant challenge to the foundry engineer. In particular, it is common for the casting yield to be much less than 100% owing to defects such as solidification white spots, stray grains arising from dendrite fragmentation and freckles.[3,4]

The possible occurrence of such 'melt related' defects – coupled with the finding that some superalloys are very much easier to cast than others – has attracted the attention of researchers to the solidification characteristics of these alloys, e.g. the partitioning of solutes between the dendrites and the interdendritic liquid which gives rise to microsegregation on the scale of the periodicity of the primary dendrite arm spacing. To describe these effects, various classical non-equilibrium microstructural equations of solidification have been derived, for example in a one dimensional (1D) element or 'half arm spacing' lying between two adjacent dendrites.[5–7] Unfortunately, at the present time the extent to which the solidification path is affected by the extent of back diffusion remains an open question in superalloy metallurgy – and it seems desirable to address this situation. In general, the analysis of the back diffusion phenomenon in alloy systems is nonetheless relatively well established from a theoretical standpoint. Brody and Flemings[8] were the first to derive an analytical model acknowledging the effect of back diffusion during solidification. Their model was later modified by Clyne and Kurz[9] and then by Ohnaka.[10] Kobayashi[11] developed an analytical solution for microsegregation in the case of parabolic solid growth for dendritic structures. The above mentioned models[5–11] pertain to binary systems. Modelling the microsegregation in binary alloys is relatively straightforward if any complications arising from non-linear liquidus and solidus lines and effects of temperature that alter the partitioning coefficients are ignored. For many of the ternary systems, well established ternary phase diagrams are available,[12] which can be readily employed in microsegregation calculations. However, for quaternary or higher order systems it becomes necessary to carry out calculation of phase equilibria in conjunction with microsegregation computation to describe the solidifying system. Such a method has been employed in recent years for predicting the microsegregation in Ni based superalloys[13,14] and other alloy systems,[15–18] the procedures for calculating phase equilibria then relying upon the CALPHAD method.[19] However, such a calculation procedure is limited by the available thermodynamic databases describing the interactions between the different components of the alloy, and may not yield accurate predictions for alloy compositions lying outside the range of the thermodynamic data.

[1]Department of Materials Engineering, University of British Columbia, Vancouver, Canada, V6T 1Z4
[2]Department of Materials, Imperial College, Prince Consort Rd, London SW7 2BP, UK

*Corresponding author, email r.reed@imperial.ac.uk

Published by Maney on behalf of the Institute
Received 28 February 2005; accepted 14 July 2005
DOI 10.1179/174328406X79289

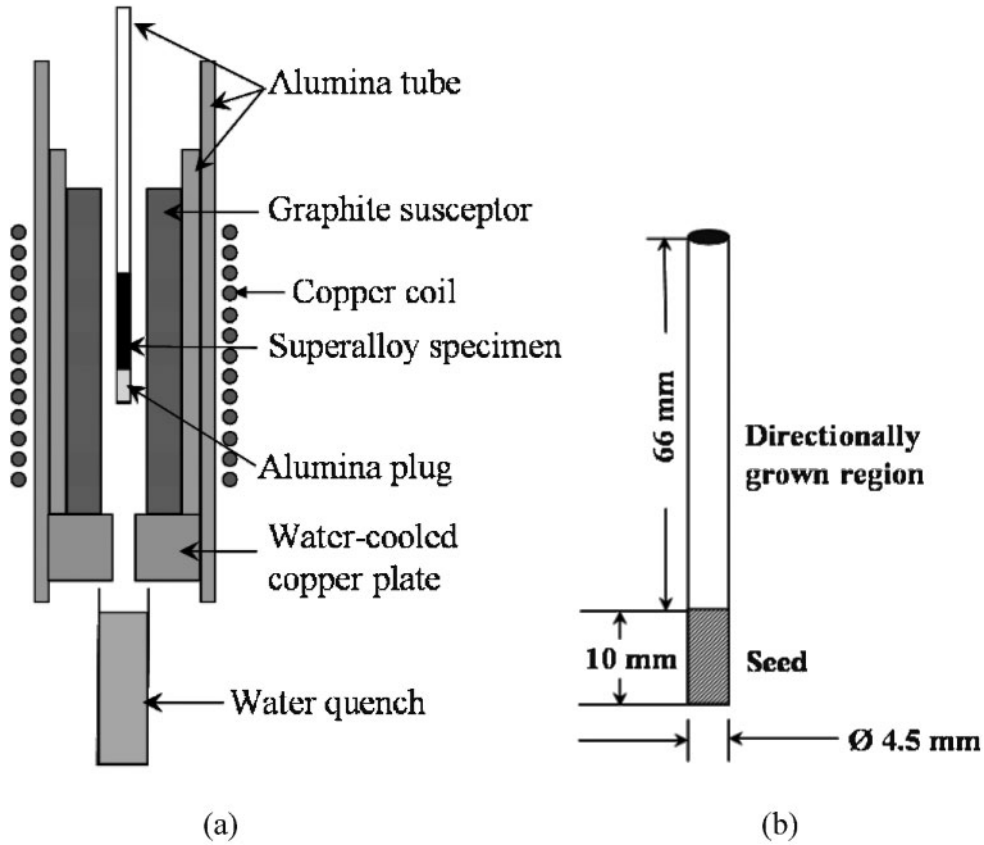

1 ***a*** **schematic illustration of DSQ furnace and** ***b*** **geometry of RR-2100 specimens used**

The purpose of the present study was twofold. First, we set out to resolve the outstanding issue concerning the extent to which back diffusion occurs during the directional solidification of a typical Ni based single crystal superalloy under conditions relevant to the investment casting process. A unique directional solidification and quenching (DSQ) furnace was used for this purpose. Second, a mathematical model of the solidification process was to be developed, which would account for the solidification path and the extent of any back diffusion that was found to occur. The present paper reports on the progress made in these respects.

Experimental

The prototype single crystal superalloy RR-2100 was supplied by Rolls-Royce in the form of cylindrical rods of 4·5 mm diameter and ~76 mm length; they had been grown using a standard investment casting method.[20] The Laue back reflection method was used to confirm that the dendrite growth direction was within a few degrees of the ⟨001⟩ crystallographic direction. The chemical composition of one of these rods was determined using Leco CS244/TC436AR furnaces and inductively coupled plasma–optical emission spectroscopy (ICP–OES). The results are shown in Table 1. It can be seen that the composition of RR-2100 is representative of the third generation single crystal superalloys that possess a Re content of ~6 wt-%.

Table 1 Chemical composition of RR-2100 alloy used in this study, wt-%

Al	Co	Cr	W	Re	Ta	Hf	Ni
6	12	2·5	9	6·4	5·5	0·15	Bal.

Differential scanning calorimetry

Differential scanning calorimetry (DSC) was used to quantify the solidification range of RR-2100. A Setaram TGA-DTA/DSC-96 instrument was used for this purpose. Cylindrical specimens of 4·5 mm diameter and 2 mm thickness were found to yield an acceptable signal to noise ratio. The measurement range was 10 to 1500°C. Measurements were made under a cooling rate of 10 K min^{-1} in an atmosphere of helium. Both the specimens and the reference crucibles employed were made of α-alumina. An α-alumina specimen of known mass and specific heat was used as the calibrant. The specific heat capacity of RR-2100 was then determined using the ratio method following standard ASTM procedures.[21] The data for specific heat *v.* temperature were converted to fraction solid *v.* temperature by determining the fractional area under the specific heat curve.[14]

Directional solidification and quenching experiments

A vertical configuration Bridgman type DSQ furnace was used to quench single crystal specimens which were growing under well controlled withdrawal rates and prescribed temperature gradients. A schematic illustration of the DSQ furnace is given in Fig. 1*a*. A small portion of each specimen, of length ~10 mm, was deliberately left unmelted during each run (*see* Fig. 1*b*), and this constituted the seed for single crystal growth. The temperature gradient in the hot zone was measured

with Type D (W–3%Re/W–25%Re) thermocouples and was $\sim$10 K mm^{-1}. A withdrawal rate of 1 mm min^{-1} was employed. After withdrawal, the specimen was quenched in a water bath located below the heating coils and water cooled copper plate, so that the solidifying microstructure was effectively frozen in. Specimens therefore prepared were characterised with Laue back reflection, and the dendrite orientation was confirmed to be within 10° of the $\langle 001 \rangle$ direction.

Optical metallography

The DSQ specimens were sectioned longitudinally close to the dendrite growth direction and prepared for optical metallography. An example of the microstructure in one of the specimens can be seen in Fig. 2; this provides visual confirmation of the directionally solidified structure. Additionally, average primary dendrite arm spacings were estimated by measuring the dendrite core to dendrite core distance for a number of dendrites. These measurements were repeated on transverse sections to verify the validity of the measurements made on the longitudinal sections. The results were not found to be substantially different when repeated in this way. Primary dendrite spacings were found to be $\sim$250 μm at the withdrawal rate of 1 mm min^{-1}.

Electron probe microanalysis experiments

The longitudinally sectioned specimens were polished to a 1 μm finish and coated with graphite for analysis of composition using a Cameca SX-50 electron probe microanalyser (EPMA). Measurements were made along horizontal lines (normal to the solidification direction) in the mushy zone of a RR-2100 specimen solidified under a temperature gradient of 10 K mm^{-1} and a withdrawal speed of 1 mm min^{-1}(*see* Fig. 3*a*). These point scans were carried out over a region of 6000×3000 μm at a regular spacing of 20 μm in the transverse direction and every 300 μm in the solidification direction; other than to align the regular mesh parallel and perpendicular to the solidification direction, it was placed at random on the microstructure. A second set of point scans were also carried out at locations corresponding to the dendrite centres and interdendritic regions alone (*see* Fig. 3*b*). Wavelength dispersive spectrometers (WDS) were employed in the microprobe which were equipped with crystals of LIF (for detection of Cr, Co, Ni and Re peaks), TAP (for detection of Al and Ta peaks) and PET (for detection of W peaks).[22] X-ray peaks and backgrounds were recorded simultaneously for Al K_α, Co K_α, Cr K_α, Ta M_α, W M_α, Re L_α and Ni K_α. The peaks from the specimens were compared with those from pure element standards and converted to concentration values using standard correction procedures.[22,23] Hafnium, which was present only in trace quantities, was not considered in the analysis. Table 2 summarises the parameters used for the scans.

Because the point scans were made normal to the solidification direction traversing a distance equivalent to at least 20 dendrite arms – with the measurement points equally spaced along it – each set is then representative of the entire range of solid fractions at any given depth in the mushy zone. Nonetheless, the statistical noise in the data is likely to be significant (given that the measurement points were made at random) and therefore a sorting algorithm was employed to derive the relationship between local

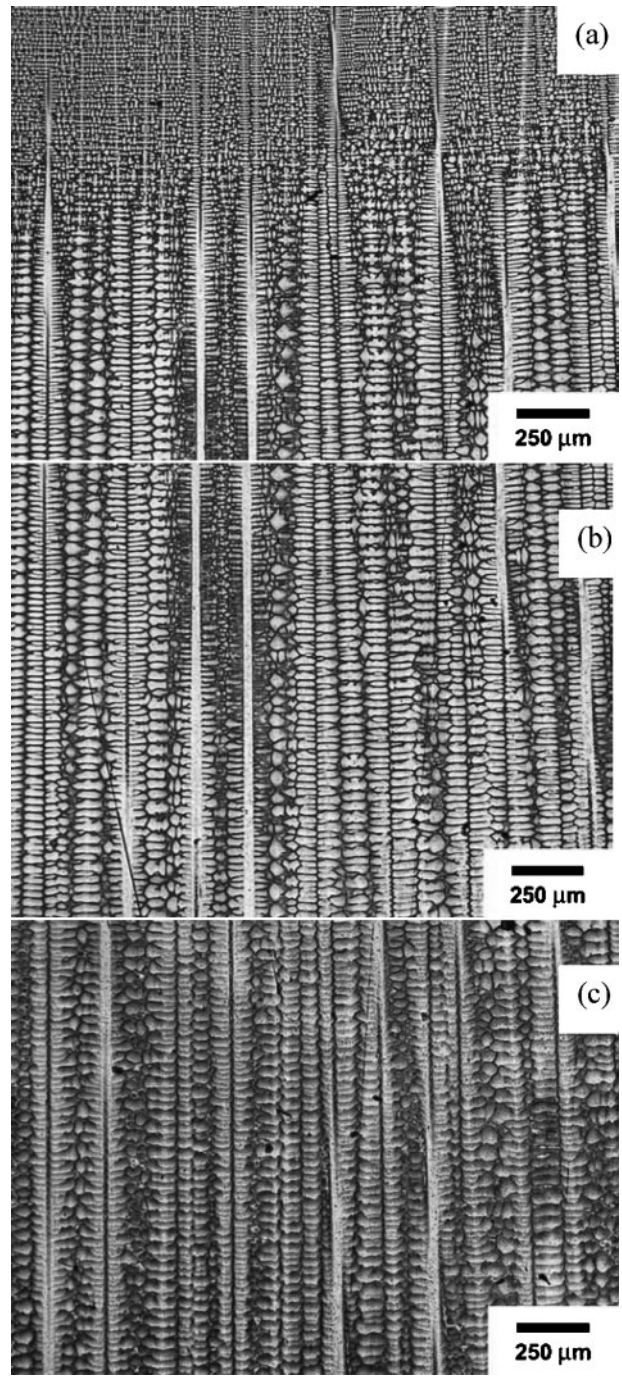

a top of mushy zone; *b* middle of mushy zone; *c* bottom of mushy zone

2 Microstructure of mushy zone of directionally solidified RR-2100

Table 2 Parameters employed for EPMA scans

Beam current, nA	Accelerating voltage, kV	Take-off angle, °	Counting time. s	Beam size, μm
40	20	40	63	5

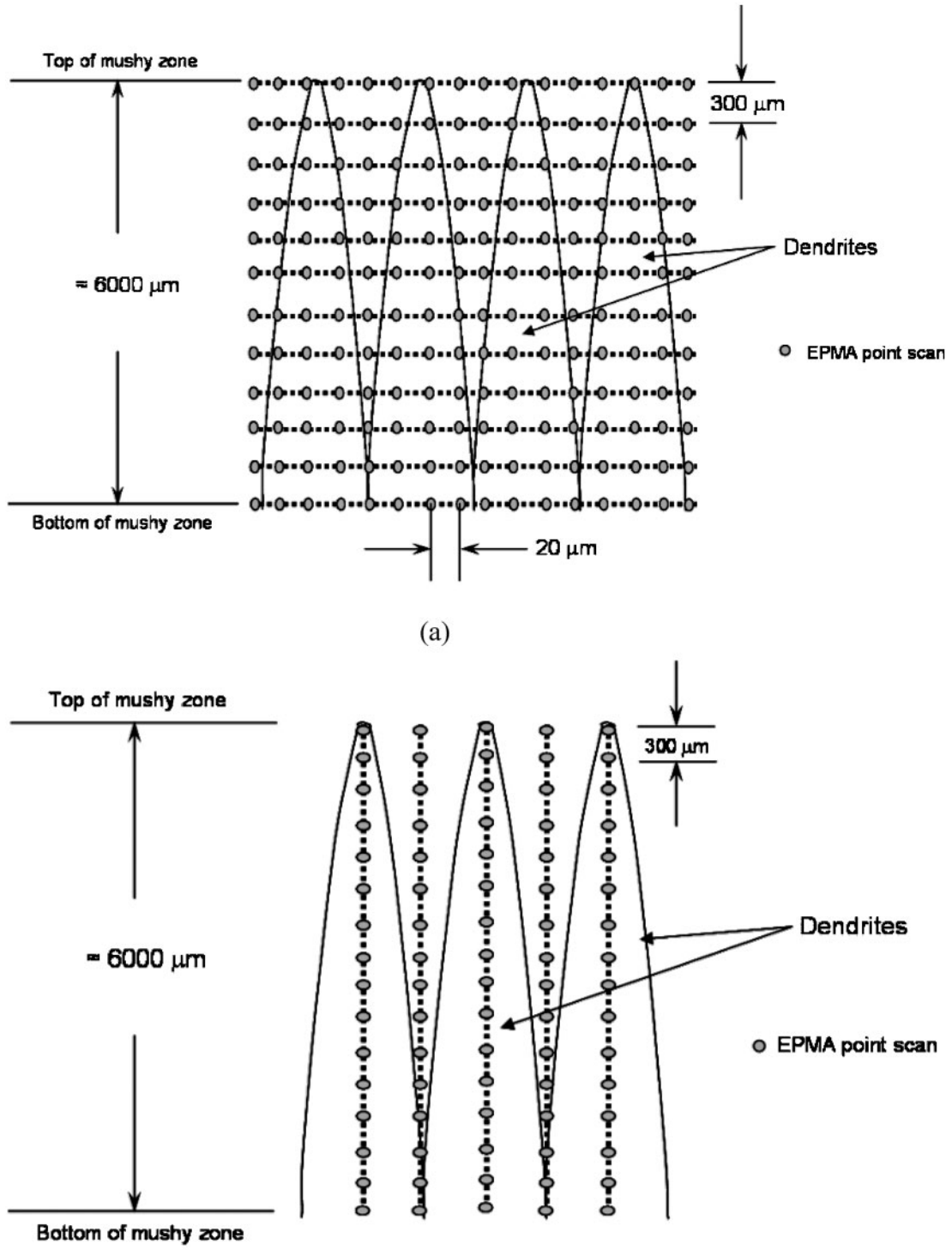

a scans made transverse to solidification direction; *b* scans made in solidification direction at dendrite centres and inter-dendritic regions

3 Schematic illustration of locations used for compositional analyses in EPMA scans

concentration and fraction solidified. Because for superalloys in general (and for RR-2100 in particular, as will be described below) Re and Ta partition in different directions, the magnitude of the local quantity $(C_{Ta}-C_{Re})$ can be used as a basis for estimating the fraction f_s to which it corresponds; here C_i refers to the concentration in wt-% of the element i. The procedure employed involved:

(i) sorting the data points into ascending order on the basis of the local value of $(C_{Ta}-C_{Re})$

(ii) the assignment of an integer i lying between unity and N on this basis, where N is the total number of data points measured, and the quantity f_s placed equal to $(i-1)/(N-1)$ which is then assumed to equate to the fraction solidified at this point

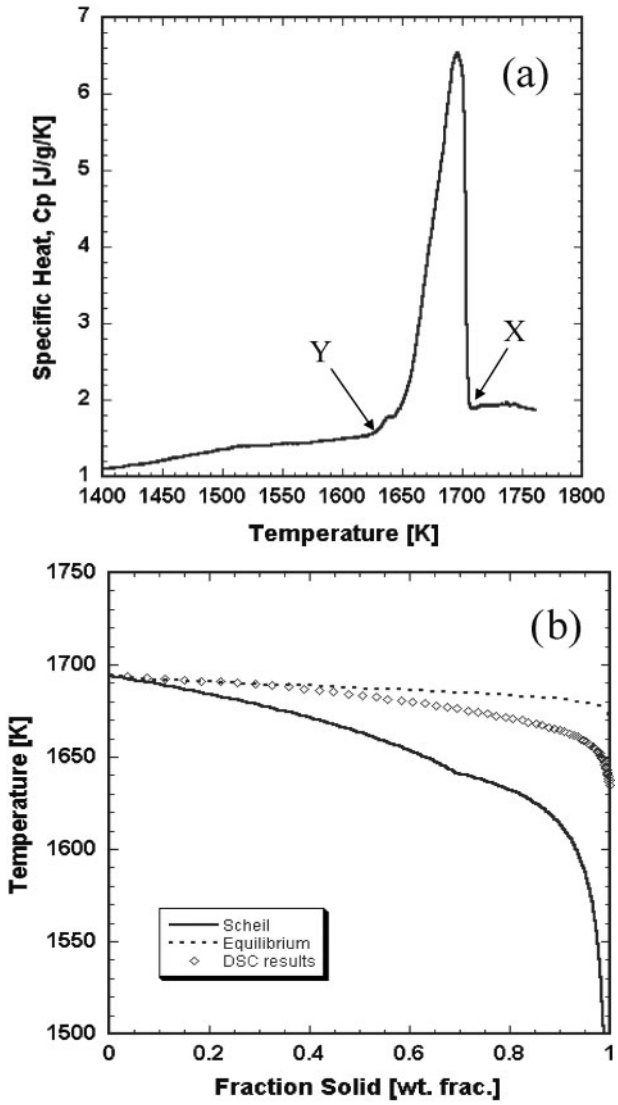

4 ***a*** **plot of specific heat capacity** ***v.*** **temperature during solidification for alloy RR-2100; symbols X and Y mark liquidus and solidus respectively and** ***b*** **variation of solid fraction with temperature as determined from DSC data**

(iii) the computation of mean concentration values within intervals of f_s corresponding to 0·02.

Results and discussion

DSC results

The specific heat capacity of RR-2100 as a function of temperature as determined by the DSC method is given in Fig. 4*a*. The solidification range was estimated as 77 K, the solidus and liquidus temperatures being 1633 and 1710 K respectively. Conversion of the data from specific heat *v.* temperature to fraction solid *v.* temperature yielded the solidification path of the alloy (Fig. 4*b*). The DSC results indicated that any eutectic reaction occurring – as suggested by the minor shoulder on the curve of Fig. 4*a* – was only a minor proportion of the overall solidification reaction; this was later confirmed by metallographical examination.

It can be seen that the path as determined by DSC lies intermediate between the Scheil and lever rule predictions, which were made using a thermodynamic database of parameters[24] operated upon by the Thermocalc software.[25] This is a first indication that back diffusion is occurring, because the solidification path departs considerably from the Scheil limit, particularly at the later stages of solidification.

EPMA measurements of composition

Attention is focused on the solidification conditions corresponding to a withdrawal rate of 1 mm min^{-1} at a temperature gradient of 10 K mm^{-1}, which is representative of the casting conditions experienced in a typical industrial scale investment casting furnace.[20] The sorting method that was employed allowed estimates to be made of the partitioning coefficients k for the different solute elements, according to

$$k = \lim_{f_S \to 0} \frac{C_S}{C_l} = \frac{C_S|_{f_S=0}}{C_0} \quad (1)$$

where C_S, C_l and C_0 are the solid, liquid and bulk compositions, respectively, and f_S is the fraction solidified. The partitioning coefficients determined in this way are given in Table 3. The values are found to be comparable with those reported elsewhere[19,26–28] for the single crystal superalloys. It can be seen that Co and Cr have partitioning coefficients close to unity and therefore do not show a marked preference for partitioning to either the solid or the liquid phases. However, Al and Ta partition strongly to the liquid while Re and W do so to the solid.

Figures 5 and 6 show the sorted compositional data for the solutes Re, Al, W and Ta plotted versus fraction solid, corresponding to distances of 6000 and 300 μm from the dendrite tips – note that the solid and broken lines are computed from the model which is described below. The experimental plots represent solute profiles within a typical 1D element lying transverse to the solidification direction, such that f_S=0 corresponds to the dendrite cores while f_S=1 corresponds to the midpoint between two adjacent dendrites. Because the alloy specimen was directionally solidified and then quenched, the extent of solidification increases towards the limit of f_S=1 with distance from the dendrite tips. To estimate the extent of solidification to which Figs. 5 and 6 correspond, it should first be noted that the temperature at any given depth in the mushy zone is given approximately by the relationship (which neglects dendrite tip undercooling)

$$T_d = T_L - dG \quad (2)$$

where T_d is the temperature at distance d from the dendrite tips, T_L the liquidus temperature and G the temperature gradient. The total fraction solidified at any given distance from the dendrite tips can then be determined from the f_S *v.* T plot in Fig. 4*b*. The solid

Table 3 Equilibrium partitioning coefficients determined for alloy RR-2100

Element	Partitioning coefficient *k*
Al	0·78±0·04
Re	1·66±0·03
Ta	0·67±0·09
W	1·47±0·06
Co	1·09±0·02
Cr	1·0±0·08

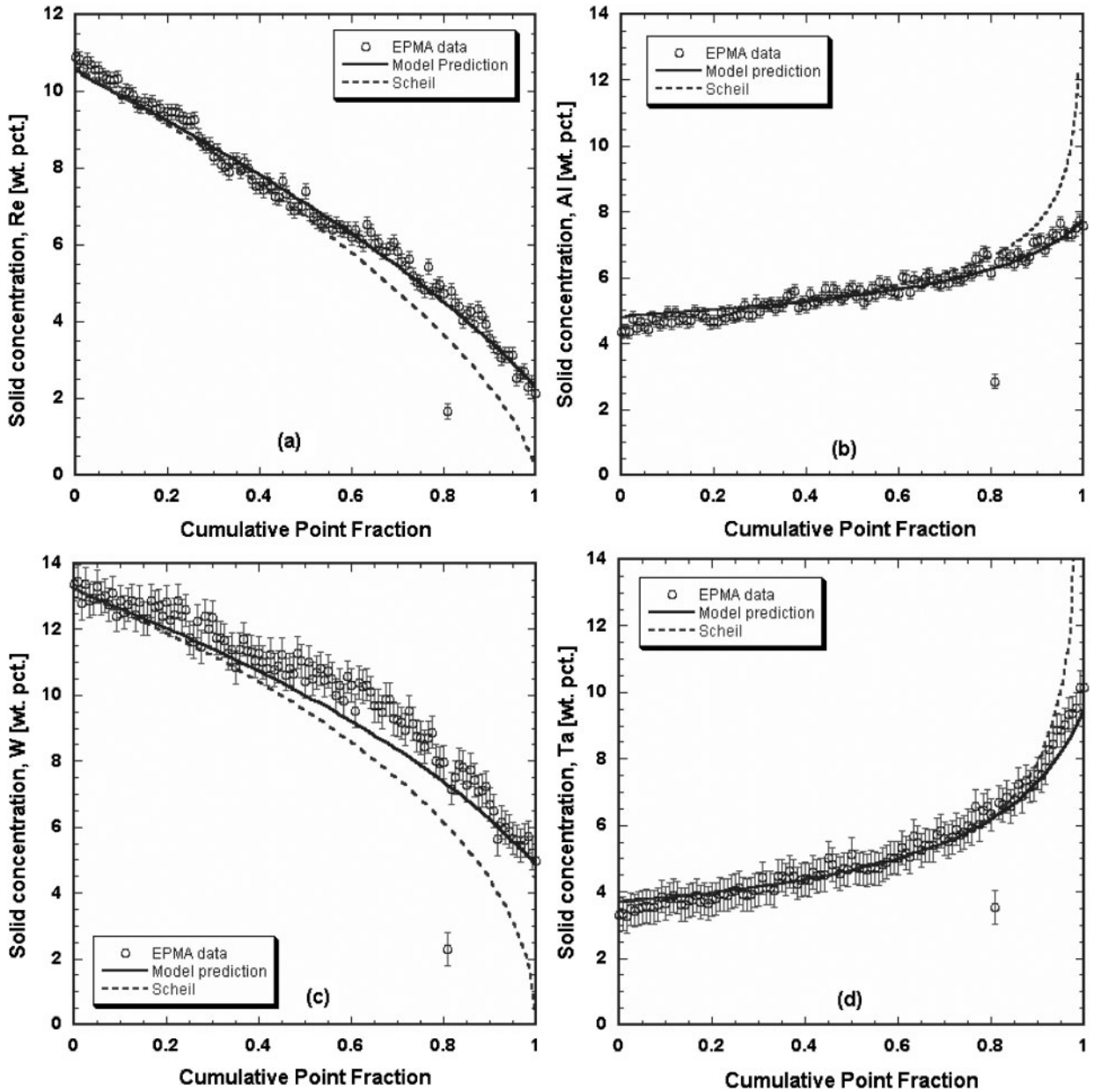

a rhenium; *b* aluminium; *c* tungsten; *d* tantalum

5 Plots showing sorted EPMA compositional data at distance of 6000 μm from dendrite tips. Also shown are model's predictions for solute profiles within volume element and predictions in Scheil limit

fractions at distances of 6000 and 300 μm from the dendrite tips were therefore estimated to be 0·99 and 0·15 respectively. The data in Fig. 5 are therefore representative of the completely solidified structure; on the other hand, the sorted data in the domain $0 \leqslant f_s \leqslant 0{\cdot}15$ in Fig. 6 represent the composition of the solid in the primary dendrite arms, while the data in the domain $0{\cdot}15 \leqslant f_s \leqslant 1$ pertain to the compositions of the interdendritic regions, i.e. the secondary arms and the quenched liquid.

Figure 7 shows the compositional data from the measurements made in the dendrite centres and interdendritic regions from the top of the mushy zone (corresponding to the dendrite tips) to the bottom (corresponding to their trunks). The plots show the variation in composition of these regions with respect to Re, Al, W and Ta as a function of depth in the mushy zone. Lines are drawn through the data as a guide to the eye. As can be seen, no variation was found in the composition at the dendrite centre from the top of the mushy zone to the bottom. On the other hand, the compositions of the interdendritic regions showed a different trend. For elements such as Re and W whose partitioning coefficients are greater than unity, the composition of the frozen interdendritic liquid decreases from a value close to the bulk composition C_0 of the alloy at the top of the mushy zone, to a minimum value at $\sim$2700 μm from the dendrite tips, and then increases to a value slightly less than C_0 at the bottom of the mushy zone. On the other hand, for elements such as Al and Ta that partition strongly to the interdendritic region, the liquid composition increases from a value close to the bulk composition C_0 of the alloy at the top of the mushy zone, to a maximum value again at $\sim$2700 μm from the dendrite tips, and then decreases to a value slightly greater than C_0 at the bottom of the mushy zone. While making scans with the microprobe it was observed that at distances less than $\sim$2700 μm from

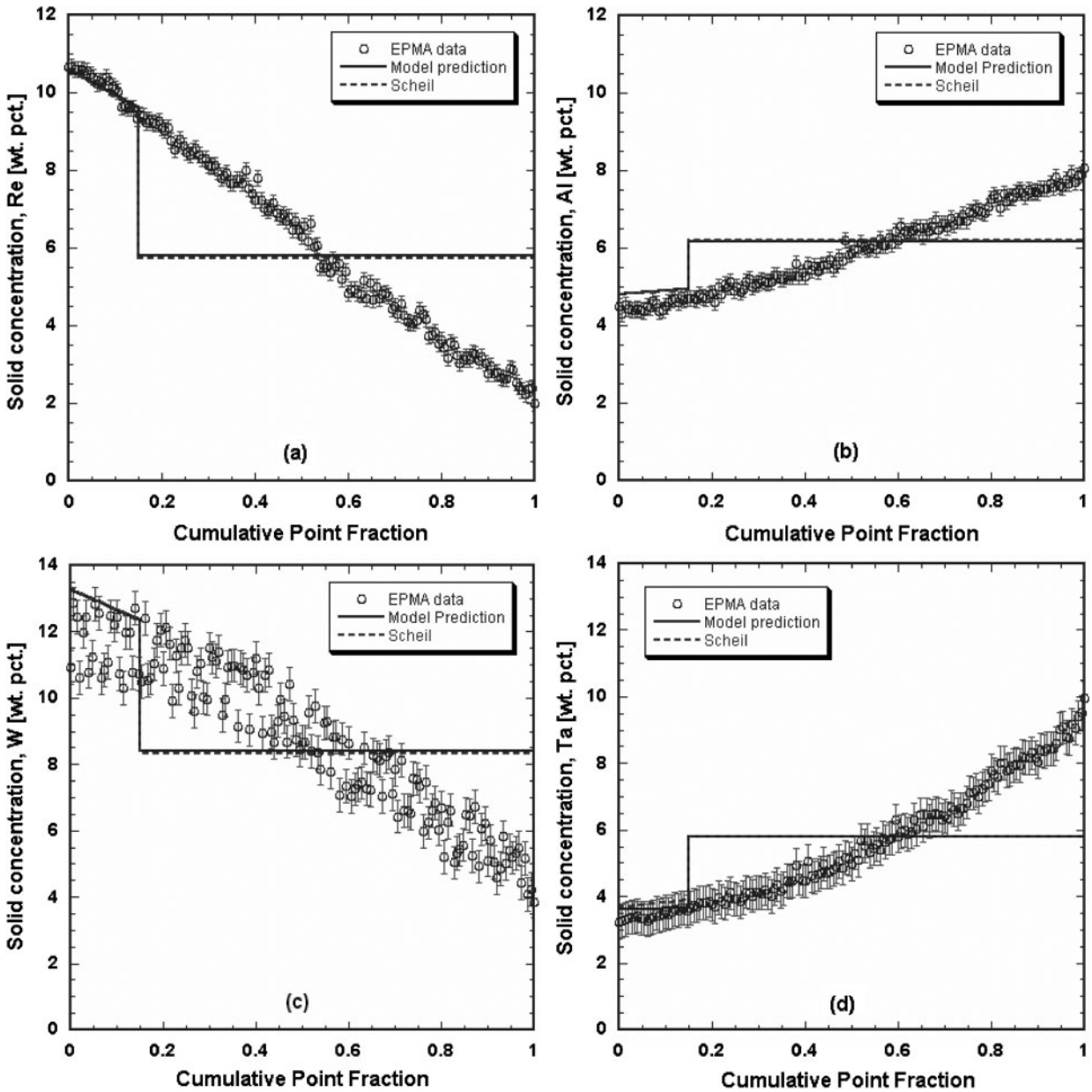

a rhenium; *b* aluminium; *c* tungsten; *d* tantalum

6 Plots showing sorted EPMA compositional data at distance of 300 μm from dendrite tips. Also shown are model's predictions for solute profiles within volume element and predictions in Scheil limit

the dendrite tips, it was relatively easy to locate the frozen liquid. At greater distances ($\geqslant$2700 μm), the side arms were seen to coalesce, therefore making it difficult to locate the liquid unambiguously; therefore, the measurements are likely to correspond to the composition of the secondary side arms rather than the frozen liquid, which would be greater than the corresponding liquid compositions by a factor approximately equal to the partitioning coefficient k. This results in the reversal in the compositional profiles beyond a depth of $\sim$2700 μm (Fig. 7); the authors do not believe that this effect is due to any effect of back diffusion or homogenisation of the compositional profiles post-solidification, although more work is required to confirm this.

Rationalisation of results

In order to analyse the sorted EPMA data for evidence of back diffusion, a model for the solidification process was developed to enable the composition within the primary arms to be examined in the domain $0 \leqslant f_s \leqslant f_s^*$, with f_s^* being the position of the planar solid/liquid interface in the volume element. The model, which is based upon the approach developed by Voller,[29] relies upon a modification of the basic Scheil approach but with back diffusion in the solid accounted for; coarsening of the dendrite arms was not considered.

Complete details of the analysis are given in the appendix; only the pertinent points will be given here together with some discussion concerning the parameters used in the modelling – these were found to be of overriding importance. Unfortunately, the thermodynamic database of parameters[24] employed by Thermocalc was found to be incapable of reproducing the experimental data with complete accuracy; short of reworking the database (which was considered beyond the scope of the present work), it was therefore not considered desirable to build a model for

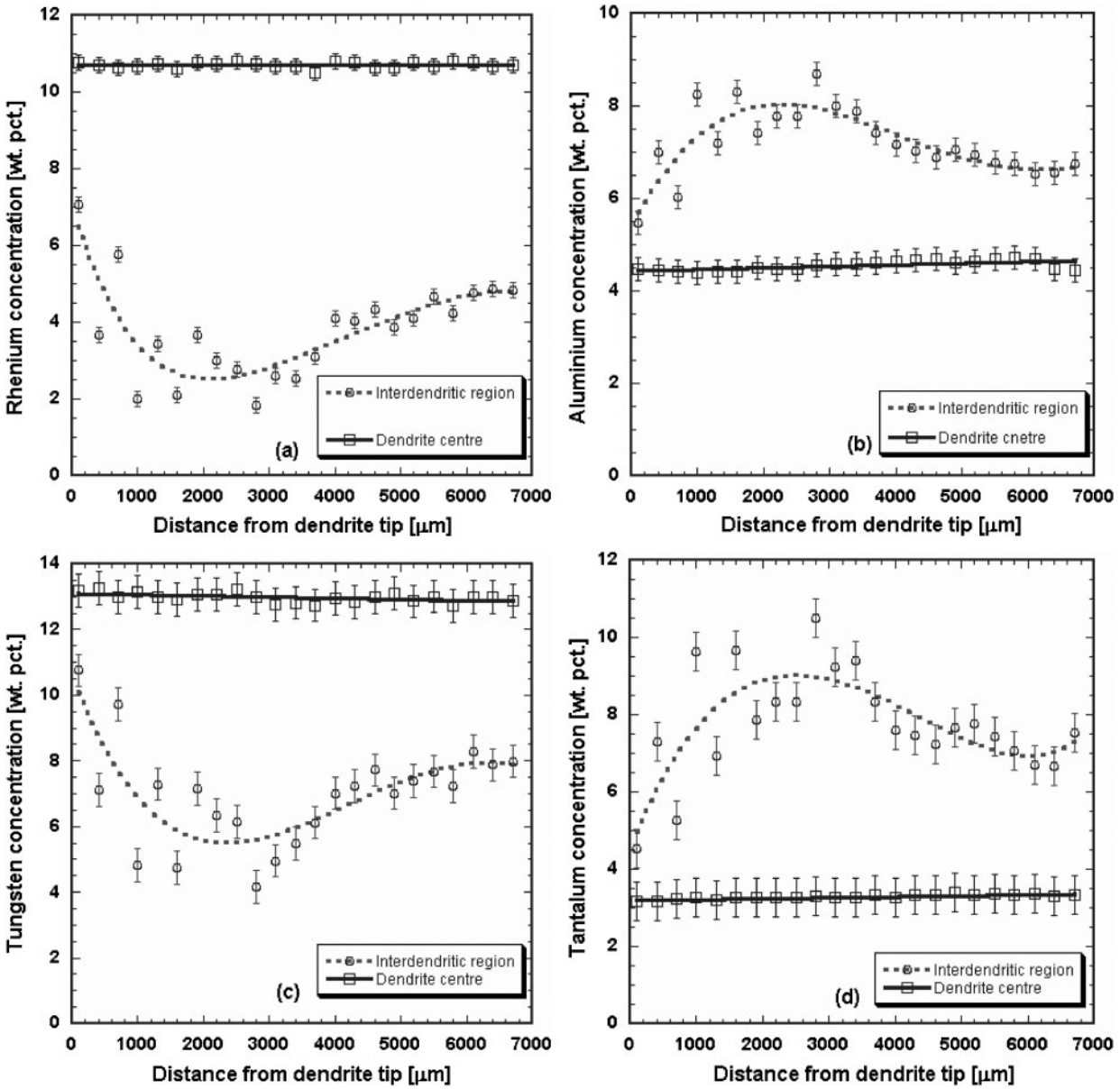

a rhenium; *b* aluminium; *c* tungsten; *d* tantalum

7 Plots of EPMA point scans showing variation in composition of interdendritic regions and dendrite centres with depth into mushy zone in RR-2100 for G=10°C mm^{-1}, V=1 mm min^{-1}

microsegregation that was fully coupled to the Thermocalc software. Instead, partitioning coefficients for the different elements were taken as constant during solidification with only the primary γ phase forming from the liquid. The dendrites were considered to be plate-like in geometry. The two halves of the primary arm spacing were taken to be identical, i.e. no mass flow was assumed to occur across the centres of the dendrite arms. Complete mixing in the liquid was assumed, while diffusion within the solid was taken to occur by volume diffusion by the standard prescription

$$\tilde{D}_{\mathrm{s}}^{\mathrm{i}} = D_0^{\mathrm{i}} \exp\left(-\frac{Q^{\mathrm{i}}}{RT}\right) \tag{3}$$

where D_0^{i} is the frequency factor term for the i^{th} solute, Q^{i} the corresponding activation energy for diffusion per mole of solute, and R the gas constant. The evolution of solid fraction during solidification was evaluated using an Euler time marching scheme on a finite difference grid according to

$$\eta_{\mathrm{s}} = \eta_{\mathrm{s}}^{\mathrm{old}} + \Delta\tau \left[\frac{\mathrm{BD}^{\mathrm{old,i}} + (1-\eta_{\mathrm{s}}^{\mathrm{old}})\,\frac{\mathrm{d}C_{\mathrm{l}}^{\mathrm{i}}}{\mathrm{d}\tau}}{(1-k^{\mathrm{i}})C_{\mathrm{l}}^{\mathrm{i}}}\right] \tag{4}$$

where η_{s} is the position of the solid/liquid interface within the volume element, $\Delta\tau$ the time step, C_{l} the liquid composition and k the partitioning coefficient. The superscript *old* refers to values at the previous time step, while the superscript i refers to the i^{th} solute. The term BD is the back diffusion term which was evaluated at the previous time step according to[29]

$$\mathrm{BD}^{\mathrm{i}} = \left(\frac{\partial C_{\mathrm{s}}^{\mathrm{i}}}{\partial\tau}\right)_{\xi} = \alpha^{\mathrm{i}}\,\frac{\partial^2 C_{\mathrm{s}}^{\mathrm{i}}}{\partial\eta^2} + \left[\frac{\eta}{\eta_{\mathrm{s}}(\tau)}\,\frac{\mathrm{d}\eta_{\mathrm{s}}}{\mathrm{d}\tau}\right]\,\frac{\partial C_{\mathrm{s}}^{\mathrm{i}}}{\partial\eta} \tag{5}$$

The parameter ξ is the normalised space variable in a Landau transformed domain representing the solid in the half arm spacing. The term α^{i} is the Fourier number for the i^{th} solute. The scheme was solved iteratively and

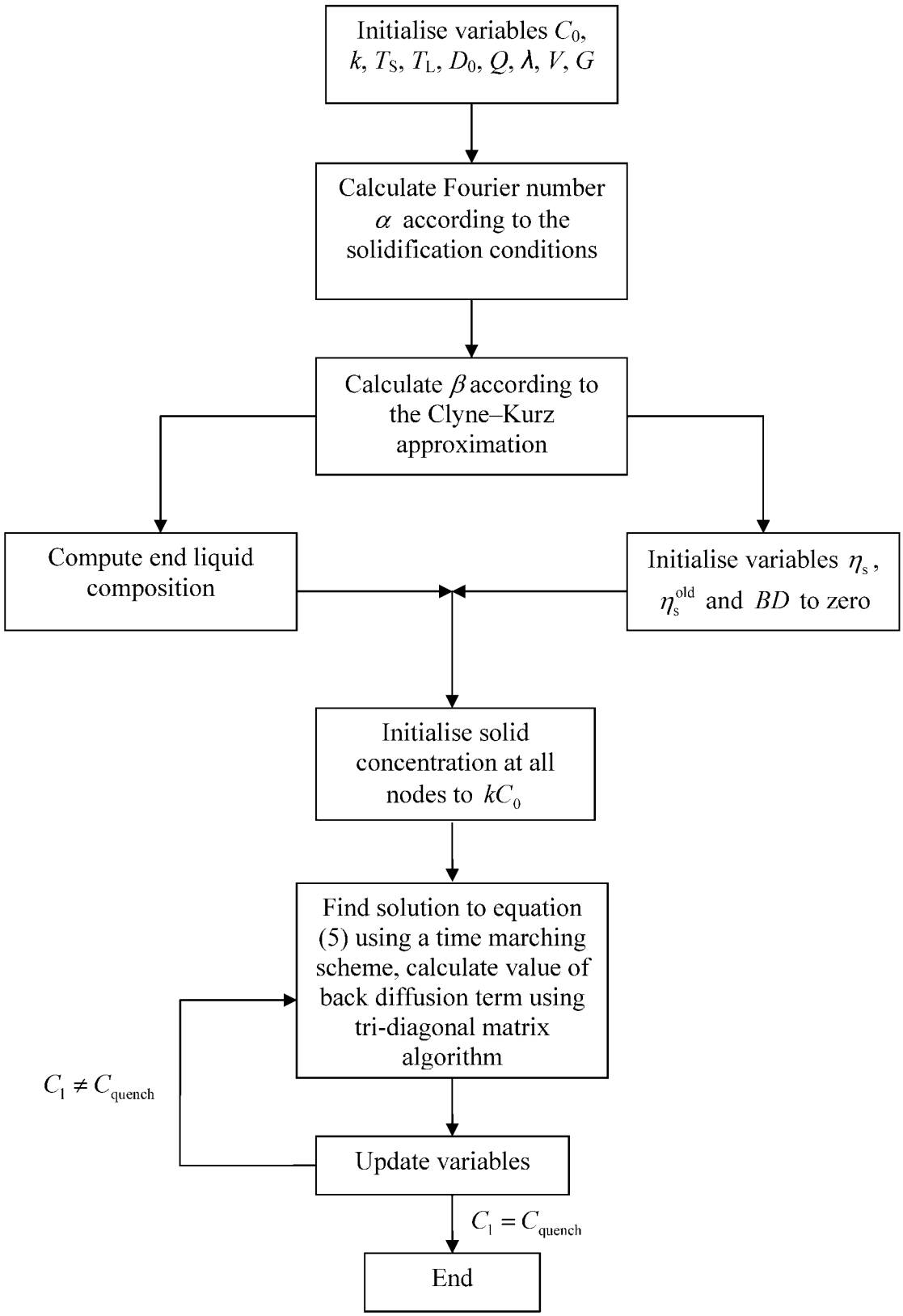

8 Flowchart showing calculation procedures used in model

the values of the different variables updated at the end of each time step. Figure 8 shows a flowchart illustrating the calculation procedure. The partitioning coefficients in Table 3 (i.e. those found in the present work) were used in the model. The data for diffusivity of the four elements segregating most, namely, Al, Re, Ta and W, were taken from the literature and are given in Table 4. The diffusivities of the different elements were calculated at each time step with decreasing temperature, and the Fourier number was evaluated. The Clyne and Kurz approximation was used to replace α^i in equation (5).

In order to obtain solute profiles in the solid in the mushy zone at different distances from the dendrite tips, solidification was terminated at prescribed values of the solid fraction. The analysis was carried out for each of the four elements Al, Re, W and Ta at different

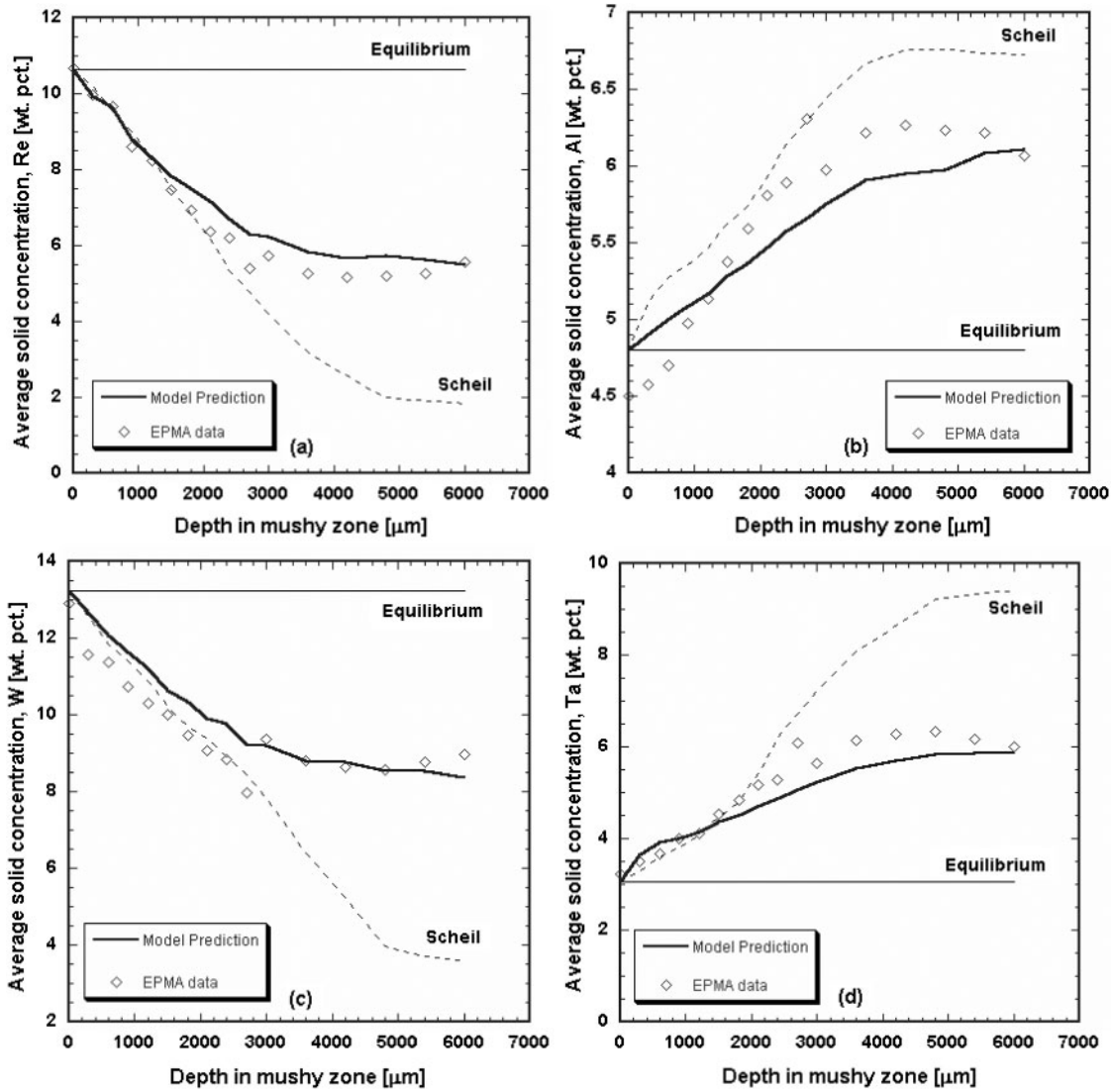

a rhenium; *b* aluminium; *c* tungsten; *d* tantalum

9 Plots showing variation in average solid composition in half arm spacing as function of depth in mushy zone. Limiting cases of Scheil and lever rules are also shown

distances from the dendrite tips. In a multicomponent alloy, the front velocities for the different components will be different, therefore the front velocity for the slowest diffusing solute was considered to be rate limiting, which was taken to be rhenium; and the front velocities of the other elements were fixed at the value determined for this element.

The predicted variations in solid composition in the primary dendrite arms, for the solutes Re, Al, W and Ta at depths corresponding to 6000 and 300 μm respectively, are given in Figs. 5 and 6. The model assumes that the interdendritic region consists only of the liquid phase, and the presence of secondary arms and solute redistribution therein are not considered – therefore beyond the solid/liquid interface, the model reports that the composition is uniform and equal to the composition of the liquid at the solid/liquid interface. It can be seen that the predictions of the model for the solid composition in the domain defined by $0 \leqslant f_s \leqslant f_s^*$ corresponding to the primary arms, agree well with the data at the two different depths shown. In particular, there is complete agreement with the data obtained at the bottom of the mushy zone (Fig. 5). In Fig. 6, corresponding to $f_S = 0{\cdot}15$, although the agreement is not perfect, it can be seen that the model is able to account for the composition gradients observed in the solid in the primary arms in a reasonable way.

Table 4 Diffusion coefficients and activation energies for diffusion of Al, Ta, Re and W in gamma phase from different sources

Element	D_0, $m^2\ s^{-1}$	Q, kJ mol^{-1}	Reference
Al	$7{\cdot}7 \times 10^{-3}$	342	30
Ta	$2{\cdot}19 \times 10^{-5}$	251	31
Re	$8{\cdot}2 \times 10^{-7}$	255	31
W	$8{\cdot}0 \times 10^{-6}$	264	31

Evidence for back diffusion

If back diffusion is indeed occurring in these systems during solidification, with increasing solid fraction (or alternatively with greater distance from the dendrite tips) the average solute concentration in the dendrites should alter, eventually approaching the equilibrium limit should the time for diffusion processes be sufficient. Evidence has indeed been found for this,

although the equilibrium limit is not reached. Figure 9 shows the average composition of the solid with regard to Re, Al, W and Ta in the primary arms as a function of depth in the mushy zone, calculated according to

$$\frac{\int_0^{f_S^*} C_s^i\{f_s\}\mathrm{d}f_s}{\int_0^{f_S^*} \mathrm{d}f_s} \qquad (6)$$

where the superscript i refers to one of the four solutes, Re, Al, W or Ta. The term f_s^* is the position of the planar solid/liquid interface in the volume element in the primary half arm space. The corresponding Scheil and lever rule predictions are also shown, as calculated from the model. The solid lines are the predictions of the model of microsegregation, with back diffusion accounted for. The homogenising effect of the back diffusion is readily discernible in these plots – at greater depths in the mushy zone where the time allowed for diffusion is a significant fraction of the local solidification time, the average composition of the solid in the arm space approaches a uniform value. At shorter distances from the dendrite tips however, the average values are closer to the Scheil limit. It can also be seen that both the EPMA data and predictions of the model agree reasonably well and lie between the upper and lower bounds of the lever and Scheil rules. The reasonable agreement between the modelling and experiment indicates that the magnitude of the back diffusion effect is reasonably accounted for.

Interpretation of α and k in terms of fitting parameters

Although the model predictions in Figs. 5 and 6 represent reasonably good fits to the experimental data, it should be acknowledged that the roles played by α and k are those of fitting parameters, although they are of course physically based. For example, the value of the partitioning coefficient for each element is chosen after sorting the data, and this procedure contributes to the good fit that is displayed – this is seen particularly in the limit of $f_S \rightarrow 0$ when the model predictions coincide with the experimental data.

On the other hand, for the diffusion parameter α, a sensitivity analysis is useful. Furthermore, it is interesting to deduce the 'best fit' values of the diffusivities by fitting appropriate values of the diffusion coefficients to the experimental data. Figure 10 shows a comparison between the experimental data and the predictions of the model for different values of α for Re, W and Ta. The calculations were performed for conditions at the bottom of the mushy zone, i.e. at a depth of $\sim$6000 μm, when solidification is complete. The values of the partitioning coefficients used are indicated. From these plots, estimates for the diffusivities $\tilde{D}$ of different elements were made – the values are given in Table 5.

In Fig. 11, the diffusivities for the three elements Re, W and Ta obtained in this way are reported as averages in the corresponding ranges in Table 5, and are plotted as a function of the atomic number. Also shown therein are the data of Karunaratne and Reed[32] from experimental measurements of the diffusivities obtained from diffusion couple methods. It can be seen that the estimates for the diffusivities of Re, W and Ta obtained in the present study show a similar trend at a

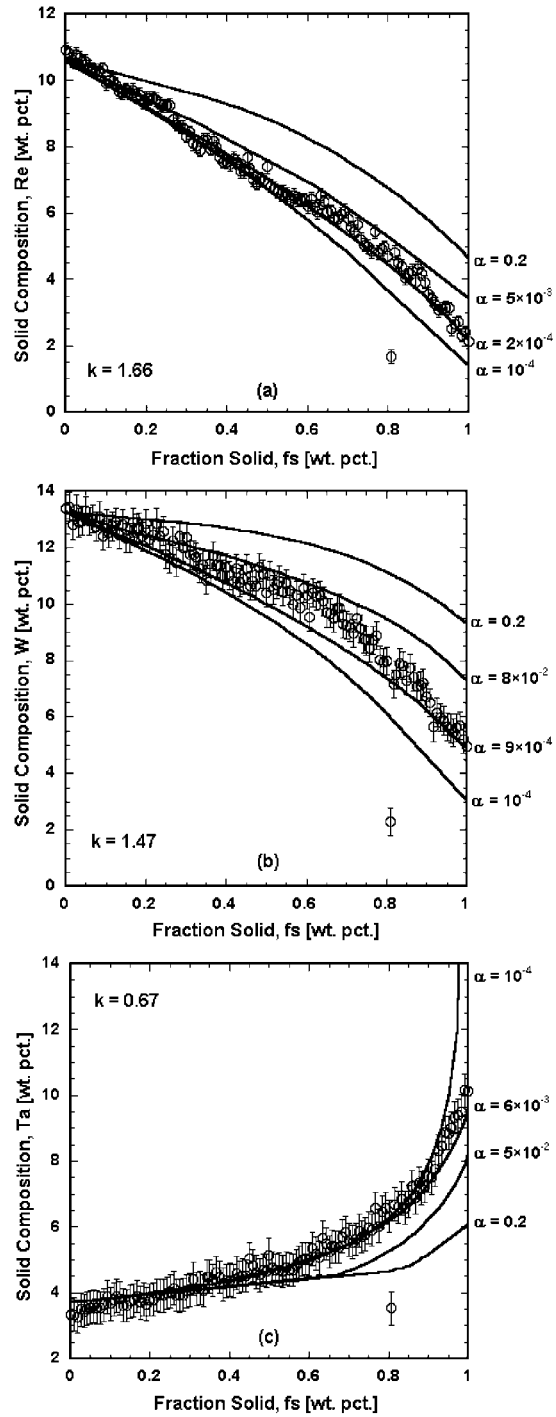

a rhenium; *b* tungsten; *c* tantalum

10 Plots showing comparison between experimental data and predictions of model for different values of α at bottom of mushy zone in RR-2100, illustrating sensitivity of model to variations in parameter α

Table 5 Range of variation in α, Fourier number for Re, W and Ta that yield values of diffusivity $\tilde{D}$ resulting in reasonable fits to experimental data from EPMA at depth of 6000 μm

Element	α	$\tilde{D}$, m^2 s^{-1}
Re	$2-3\times10^{-4}$	$6{\cdot}8\times10^{-15}-1{\cdot}0\times10^{-14}$
W	$7-9\times10^{-4}$	$2{\cdot}4\times10^{-14}-3{\cdot}0\times10^{-14}$
Ta	$5-7\times10^{-3}$	$2{\cdot}0\times10^{-13}-2{\cdot}4\times10^{-13}$

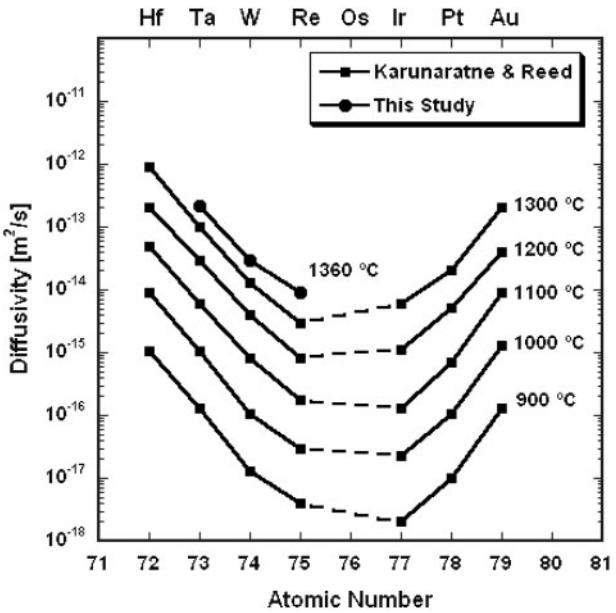

11 Plot showing diffusivity of Re, W and Ta as function of atomic number. Data points represented by circular markers are estimates obtained in present study while square markers represent data from Ref. 32

temperature of 1360°C, the solidus temperature of RR-2100, as at lower temperatures. Although the data from Ref. 32 pertain to binary diffusion couples and those deduced here correspond to the γ phase in RR-2100 that is heavily alloyed, the fact that the trends for the respective diffusivities of Re, W and Ta are preserved, i.e. $\tilde{D}_{\mathrm{Re}} < \tilde{D}_{\mathrm{W}} < \tilde{D}_{\mathrm{Ta}}$, indicates that the parameters introduced here to describe the back diffusion are of the correct magnitude and back diffusion is indeed occurring in these systems.

Summary and conclusions

The solidification characteristics of the experimental rhenium containing third generation single crystal superalloy RR-2100 were examined. Differential scanning calorimetry indicated that the solidification range for this alloy is 77 K, the liquidus and solidus temperatures being 1710 and 1633 K respectively – a temperature interval too large for back diffusion to be completely absent, as indicated by equilibrium and Scheil calculations made with a thermodynamic database. To investigate this further, DSQ experiments were carried out to 'freeze in' the solidifying microstructure, which was then characterised with EPMA analysis; a statistical treatment of the datasets allowed the solidification path to be estimated in the 1D element defined by the midpoint between adjacent dendrite arms and the dendrite core. The partitioning coefficients for the different alloying elements were estimated from this procedure and were found to be in agreement with previously reported values. The results were compared with a solidification model that accounted for back diffusion, and evidence for back diffusion in the primary dendrites in the mushy zone was found – the average composition of the solid in the mushy zone approached a uniform value, confirming the homogenising effect of back diffusion. The average solid concentrations of aluminium and tantalum decreased with the depth in the mushy zone to a uniform value while those of rhenium and tungsten increased. Estimates for the diffusivities of the slow diffusing Re, W and Ta solutes were obtained from the model using a sensitivity analysis. The values deduced in this way were found to be in good agreement with recent data reported in the literature, which were obtained from diffusion couple experiments.

Appendix

The solute balance in the 'half arm spacing' between the dendrite core and the midpoint between an adjacent dendrite can be written

$$\int_0^{\eta_s} C_s \mathrm{d}x + (1-\eta_s)C_l = C_0 \tag{7}$$

where η_s is the length of the solid phase in the half arm spacing, and C_s, C_l and C_0 are the solid, liquid and bulk compositions respectively.

Upon differentiating equation (7) with respect to τ, the normalised time variable is obtained

$$\int_0^{\eta_s} \frac{\partial C_s}{\partial \tau}\,\mathrm{d}\eta + (k-1)C_l\,\frac{\mathrm{d}\eta_s}{\mathrm{d}\tau} + (1-\eta_s)\,\frac{\mathrm{d}C_l}{\mathrm{d}\tau} = 0 \tag{8}$$

where k is the partitioning coefficient of the solute.

Within the solid domain $0 \leqslant \eta \leqslant \eta_s$, solute diffusion is governed by Fick's second law so that

$$\frac{\partial C_s}{\partial \tau} = \alpha\,\frac{\partial^2 C_s}{\partial \eta^2} \tag{9}$$

where $\alpha = \tilde{D}_s t_f / X_f^2$ is the Fourier number for the solute in the solid. The term $\tilde{D}_s$ is the mass diffusivity of the solute in the solid that is temperature dependent. Substituting equation (9) into (8) and rearranging, the following is obtained

$$\frac{\mathrm{d}\eta_s}{\mathrm{d}\tau} = \frac{\alpha \frac{\partial C_s}{\partial \eta}\Big|_{\eta_s} + (1-\eta_s)\,\frac{\mathrm{d}C_l}{\mathrm{d}\tau}}{(1-k)C_l} \tag{10}$$

therefore, any scheme based upon this method requires the rate of change of the liquid concentration with time to be determined; this can be estimated according to

$$\frac{\mathrm{d}C_l}{\mathrm{d}\tau} = \frac{\mathrm{d}C_l}{\mathrm{d}f_s}\,\frac{\mathrm{d}f_s}{\mathrm{d}T}\,\frac{\mathrm{d}T}{\mathrm{d}\tau} \tag{11}$$

the second term on the right hand side describes the rate of change of the solid fraction with temperature; this is evaluated by computing the slope of the curve in Fig. 4*b* at a given value of the solid fraction. The third term on the RHS is the cooling rate employed; this is known from the experimentation. Therefore

$$\frac{\mathrm{d}T}{\mathrm{d}\tau} = GVt_f \tag{12}$$

where G is the temperature gradient in the mushy zone, V the withdrawal speed, and t_f the local solidification time. The rate of the change of liquid composition with fraction solidified is given by[6]

$$\frac{\mathrm{d}C_l}{\mathrm{d}f_s} = (1-k)C_0(1-f_s)^{k-2} \tag{13}$$

where C_0 is the initial composition.

Because the local solidification time is given by

$$t_f = \frac{\Delta T_{L\to S}}{GV} \tag{14}$$

where $\Delta T_{L\to S} = T_L - T_S$ is the freezing range of the alloy. Combining equations (12), (13) and (14), equation (15*a*) can be given as

$$\frac{dC_l}{d\tau} = (1-k)C_0(1-f_s)^{k-2}\frac{df_s}{dT}\Delta T_{L\to S} \tag{15a}$$

the end liquid composition C_{quench} varies with the distance from the dendrite tips and defines the liquid composition at which solidification is terminated by quenching. This can be evaluated at the solidification termination point as

$$C_{quench} = C_0 + \frac{dC_l}{d\tau} n\Delta\tau \tag{15b}$$

where n is the number of time step iterations performed before the termination solidification point is reached, and $\Delta\tau$ is the time step size. An Euler treatment after combining equations (15*a*) and (10) gives

$$\eta_s = \eta_s^{old} + \Delta\tau\left[\frac{BD^{old} + (\eta_0 - \eta_s^{old})\frac{dC_l}{d\tau}}{(1-k)C_l}\right] \tag{16}$$

where the term BD is a back diffusion parameter given by $BD = \alpha(\partial C_s/\partial\eta)$.

The front is fixed in space in the usual way using a Landau transformation so that[29]

$$\left(\frac{\partial C_s}{\partial\tau}\right)_\xi = \alpha\frac{\partial^2 C_s}{\partial\eta^2} + \left[\frac{\eta}{\eta_s(\tau)}\frac{d\eta_s}{d\tau}\right]\frac{\partial C_s}{\partial\eta} \tag{17}$$

which describes the changing solute concentration in the solid with time. The solid domain defined by $0 \leqslant \xi \leqslant 1$ remains fixed in time. Equation (17) is subject to the boundary conditions[29]

$$\left.\frac{\partial C_s}{\partial\eta}\right|_{\eta=0} = 0, \text{ and } C_s|_{\eta=\eta_s} = kC_l(\tau) \tag{18}$$

and the initial condition

$$C_l = C_0 \tag{19}$$

equation (17) is solved using a tridiagonal matrix algorithm and the back diffusion term evaluated according to a second order difference formula.

Acknowledgements

The authors acknowledge funding from NSERC (Canada) and the Canada Research Chair program that supports RCR's position at the University of British Columbia. The authors are also grateful to Professor Alec Mitchell for helpful discussions, to Mr Rudy Cardeno for technical support and to Bob Broomfield of Rolls-Royce plc for the provision of the RR-2100 alloy used in the present study.

References

1. K. A. Green, T. M. Pollock, H. Harada, T. E. Howson, R. C. Reed, J. J. Schirra and W. S. Walston (eds.): Proc. 10th Int. Conf. on 'Superalloys', Warrendale, PA, 2004, The Minerals, Metals and Materials Society (TMS).
2. P. R. Beeley and R. F. Smart (eds.): 'Investment casting'; 1995, London, The Institute of Materials.
3. C. Beckermann, J. P. Gu and W. J. Boettinger: *Metall. Mater. Trans.*, 2000, **31**, 2545.
4. P. Aubertin, T. Wang, S. L. Cockcroft and A. Mitchell: *Metall. Mater. Trans.*, 2000, **31**, 801.
5. G. H. Gulliver: *J. Inst. Met.*, 1913, **9**, 120.
6. E. Z. Scheil: *Metallurgy*, 1942, **34**, 70.
7. W. G. Pfann: *Trans. AIME*, 1952, **194**, 747.
8. H. D. Brody and M. C. Flemings: *Trans. AIME*, 1966, **236**, 615.
9. T. W. Clyne and W. Kurz: *Metall. Trans.*, 1981, **12A**, 965.
10. I. Ohnaka: *Trans. Iron Steel Inst. Jpn*, 1986, **26**, 1045.
11. S. Kobayashi: *Trans. Iron Steel Inst. Jpn*, 1988, **28**, 278.
12. D. R. F. West: 'Ternary equilibrium diagrams'; 1982, New York, Chapman & Hall.
13. M. C. Schneider, J. P. Gu, C. Beckermann, W. J. Boettinger and U. R. Kattner: *Metall. Mater. Trans.*, 1997, **28A**, (7), 1517.
14. M. S. A. Karunaratne, D. C. Cox, P. Carter and R. C. Reed: in 'Superalloys 2000', (ed. T. M. Pollock, R. D. Kissinger, R. R. Bowman, K. A. K. A. Green, M. McLean, S. Olson and J. J. Schirra), 263; 2000, Warrendale, PA, TMS.
15. X. Dore, H. Combeau and M. Rappaz: *Acta Mater.*, 2000, **48**, 3951.
16. X. Yan, S. Chen, F. Xie and Y. A. Chang: *Acta Mater.*, 2002, **50**, (9), 2199.
17. S. W. Chen and Y. A. Chang: *Metall. Trans.*, 1991, **22A**, (1), 267.
18. W. J. Boettinger, U. R. Kattner and S. R. Corriell: in 'Modeling of casting, welding and advanced solidification processes 1995', (ed. M. Cross and J. Campbell), 649; 1995, Warrendale, PA, TMS.
19. T. G. Chart, J. F. Counsell, W. Slough and P. J. Spencer: *Int. Met. Rev.*, 1975, **20**, 57.
20. P. Carter, D. C. Cox, C. A. Gandin and R. C. Reed: *Mater. Sci. Eng.*, 2000, **A280**, 233.
21. 'Annual book of ASTM standards', Vol. 14.02, 375; 2001, Philadelphia, PA, ASTM.
22. V. D. Scott, G. Love and S. J. B. Reed: 'Quantitative electron-probe microanalysis'; 1995, New York, Ellis Herwood.
23. J. L. Pouchou and F. Pichoir: in Proc. 11th Int. Conf. on 'X-ray optics & microanalysis', (ed. J. D. Brown and R. H. Packwood), London, ON, Canada, August 1986.
24. N. Saunders: in 'Superalloys 1996', (ed. R. D. Kissinger et al.), 101; 1996, Warrendale, PA, TMS.
25. B. Sundman: 'Summary of the modules of Thermo-calc', Thermo-Calc, Report D53, The Royal Institute of Technology, Stockholm, Sweden, 1984.
26. D. Cox: 'Characterisation of the microstructural evolution of single crystal nickel base superalloys', PhD thesis, University of Cambridge, UK, 2000.
27. U. Grafe and D. Ma: *Mater. Sci. Eng.*, 1999, **A270**, 339.
28. S. N. Tewari, M. Vijaykumar, J. E. Lee and P. A. Cureri: *Mater. Sci. Eng.*, 1991, **A141**, 97.
29. V. R. Voller: *Int. J. Heat Mass Trans.*, 2000, **43**, 2047.
30. J. Cermac and V. Rothova: *Acta Mater.*, 2003, **51**, 4411.
31. M. S. A. Karunaratne, P. Carter and R. C. Reed: *Mater. Sci. Eng.*, 2000, **A281**, 229.
32. M. S. A. Karunaratne and R. C. Reed: *Acta Mater.*, 2003, **51**, 2905.